# Introduction to B–C–N Materials

**Chee Huei Lee, Vijaya K. Kayastha, Jiesheng Wang, and Yoke Khin Yap**

**Abstract** B–C–N is an emerging material system consisting of novel nanostructures of boron (B), carbon (C), boron nitride (BN), carbon nitride ($CN_x$), boron-carbon nitride ($B_xC_yN_z$), and boron carbide ($B_xC_y$). These B–C–N materials are sometimes called as frontier carbon materials, because of their flexibility in forming materials of various types of hybridizations similar to those in the pure carbon system. This chapter provides a concise introduction on all these materials. Readers are referred to various references and other chapters compiled in this book for further reading.

## 1 Introduction

The arrangement of carbon atoms differentiates a pencil lead from a pricey diamond. Pencil leads consist of graphite where carbon atoms are $sp^2$ hybridized with three covalent bonds (σ-bond) forming the hexagonal network called graphene. These graphene sheets stack in the *ABABAB*… manner and bonded by the weak van der Waals forces. In diamonds, carbon atoms are $sp^3$ hybridized for four σ-bonds in a tetrahedral configuration. Graphite is soft, semimetallic, and dark (zero energy band gap), while diamond is super-hard, insulating, and transparent (band gap = 5.4 eV). In the past three decades, new carbon materials such as fullerenes [1] and carbon nanotubes (CNTs) [2] have attracted tremendous research interest and have lead to a Nobel Prize (Robert F. Curl Jr., Sir Harold W. Kroto, and Richard E. Smalley) [3]. Although fullerenes and CNTs are having bonding similar to graphite, they are packed into spherical and cylindrical structures, respectively. Clearly, the change of bond hybridization and molecular packing among carbon atoms can make very exciting new materials.

C.H. Lee, V.K. Kayastha, J. Wang, and Y.K. Yap (✉)
Department of Physics, Michigan Technological University, 118 Fisher Hall,
1400 Townsend Drive, Houghton, MI 49931, USA
e-mail: ykyap@mtu.edu

Y.K. Yap (ed.), *B-C-N Nanotubes and Related Nanostructures*,
DOI: 10.1007/978-1-4419-0086-9_1, 

Materials in the boron nitride (BN) system are structurally similar to the carbon solids. We have *hexagonal* phase-BN (*h*-BN), *cubic* phase-BN (*c*-BN), and BN nanotubes (BNNTs), which are analogous to the graphite, diamonds, and CNTs, respectively. For comparison, the bond lengths of carbon and BN materials are listed in Table 1. As shown, C–C and B–N bonds are quite close in bond lengths. However, these carbon and BN materials have different physical properties. For instance, graphite is a conductor, while *h*-BN is an insulator. Hybridization of the carbon and BN phases is predicted to create another series of novel materials called boron carbon-nitride (BCN or $B_xC_yN_z$) with physical properties intermediate to that of their precursors [10]. It is possible to tune the physical properties of these hybrids by controlling their atomic compositions.

Materials within the B–C–N triangular zone offer new vistas for materials research. They include bulks, thin films, nanotubes, and new nanostructures of carbon, boron, or compounds constructed of multiple elements using B, C, and N atoms: the smallest atoms that can form the strongest covalent bonds in solids. These materials are sometimes called as frontier carbon materials because of their flexibility to form various covalent bonds such as those in pure carbon solids [11]. Figure 1 summarizes all possible materials within the B–C–N triangular zone. Clearly, the ability to control bond hybridization, molecular packing, and composition of these materials is important to create new materials. They could possibly be useful for protective coatings, high-power electronics, nanoelectronic, and nanoscale

**Table 1** Bond lengths for $sp^2$ and $sp^3$ hybridization carbon and boron nitride (BN) bonds [4-9]

| | Bond lengths/nm | | |
|---|---|---|---|
| Bonds | $sp^2$ | $sp^3$ | between two hexagonal plane |
| C-C | 0.142 | 0.154 | 0.355 |
| B-N | 0.145 | 0.157 | 0.334 |

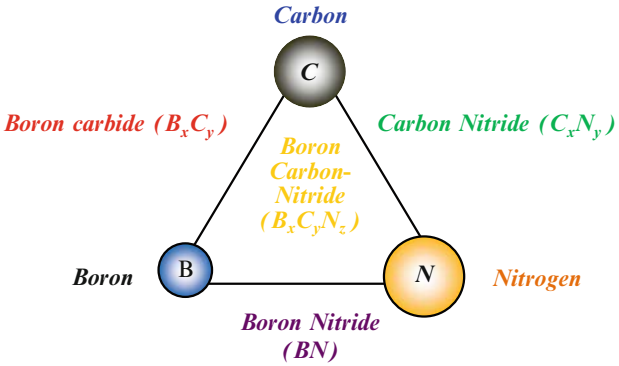


**Fig. 1** The B–C–N ternary material system

sensing devices, which are indispensable materials for nanotechnology and the advancement of science in the twenty-first century.

In this chapter, a brief introduction on carbon, BN, boron, boron carbide, carbon nitride ($CN_x$), and $B_xC_yN_z$ materials is presented.

## 2 Carbon

Carbon is the sixth element in the periodic table, and is the lightest element in the group IV of the periodic table. A carbon atom has a total of six electrons out of which four are in the valence bands. The electronic configuration of a carbon atom can be written as $1s^2 2s^2 2p^2$. In carbon, orbital energy difference between *2s* and *2p* orbitals is small in comparison to the energy released during bond formation. So *2s* and *2p* orbitals can intermix with each other during the bond formation process. This phenomenon is known as hybridization. If one "*s*" orbital mixes with *n* number of "*p*" orbitals, then it is called $sp^n$ hybridization where $n = 1, 2, 3$. These hybridized orbitals possess different geometrical shape. For example, $sp^1$ hybridized orbital has linear shape, $sp^2$ possesses trigonal planar shape, and $sp^3$ possesses tetrahedral symmetry.

Because of the flexibility in forming various type of hybridization, carbon can appear in several allotropes including the well known graphite, diamonds, and amorphous carbon. We will briefly introduce graphite, diamonds, $C_{60}$, graphene, and CNTs as examples. In particular, we will discuss a few aspects of CNTs with more details since it is the basis of other form of nanotubes to be discussed in other chapters of this book.

### *2.1 Graphite and Graphene*

Graphite is a soft carbon allotrope, which is made of sheets of hexagonal carbon networks. These carbon sheets are known as graphene. As shown in Fig. 2a, graphene sheets in graphite are stacked in a *ABAB…* sequence or Bernal stacking. In this arrangement, alternate planes are shifted relative to each other. The in-plane distance between two nearest carbon atoms ($a_{c-c}$) is 1.42 Å, and the in-plane lattice constant ($a_o$) is 2.462 Å (in-plane distance between two alternative carbon). The *C*-axis lattice constant ($c_0$) is 6.708 Å (out-of-plane distance between two alternative graphene sheets). These graphene sheets are separated by the interlayer spacing of $c_0/2 = 3.354$ Å. As we have discussed, carbon atoms within a graphene sheet are $sp^2$ hybridized. These carbon bonds are stronger than those $sp^3$ bonds in diamonds. Free carbon atom (C) will have six electrons occupied the *1s*, *2s*, $2p_x$, and $2p_y$ orbitals. The hybridized carbon atom ($C^*$) in graphite will have their electrons occupied at *1s*, three $sp^2$, and one $2p_z$ orbitals. These electronic configurations are shown as follows:

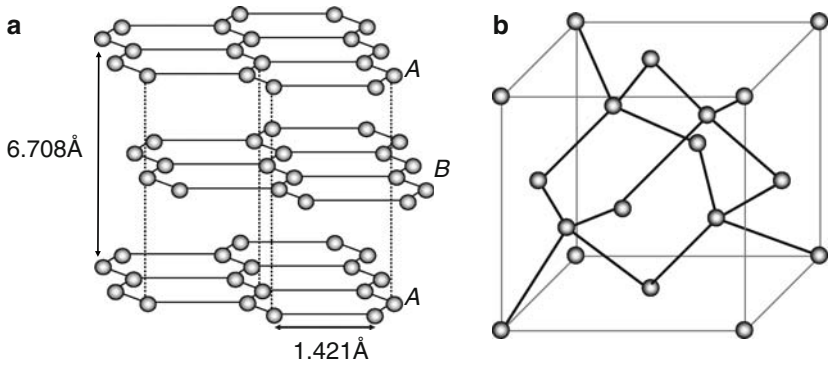


**Fig. 2** Crystal structures of (**a**) graphite and (**b**) diamonds

$$\mathrm{C}\,\frac{\uparrow\downarrow}{1s}\,\frac{\uparrow\downarrow}{2s}\,\frac{\uparrow}{2p_x}\,\frac{\uparrow}{2p_y}\,\frac{}{2p_z} \rightarrow \mathrm{C}^{*}\,\frac{\uparrow\downarrow}{1s}\,\frac{\uparrow}{sp^2}\,\frac{\uparrow}{sp^2}\,\frac{\uparrow}{sp^2}\,\frac{\uparrow}{2p_z}$$

The three electrons in the $sp^2$ orbitals are involved in the strong in-plane σ-bonds with a uniform bond angle (120°). The electrons in the $2p_z$ orbitals will form delocalized π-bonds and are responsible for the electrical conductivity of graphite. Because of the small overlapping of valence and conduction band (0.04 eV), graphite are semi-metals and have fewer charge carriers than metals. The softness of graphite arises from the weak van der Waals forces between adjacent graphene sheets.

## *2.2 Diamond*

Diamond is the hardest known material on earth. Carbon atoms in diamonds are bonded with $sp^3$ hybridization and packed in a face-centered cubic (fcc) lattice. The electronic configuration of ground state carbon (C) and $sp^3$ hybridized carbon ($C^*$) are shown as follows:

$$\mathrm{C}\,\frac{\uparrow\downarrow}{1s}\,\frac{\uparrow\downarrow}{2s}\,\frac{\uparrow}{2p_x}\,\frac{\uparrow}{2p_y}\,\frac{}{2p_z} \rightarrow \mathrm{C}^{*}\,\frac{\uparrow\downarrow}{1s}\,\frac{\uparrow}{sp^3}\,\frac{\uparrow}{sp^3}\,\frac{\uparrow}{sp^3}\,\frac{\uparrow}{sp^3}$$

The hardness of the diamond is attributed to the strength of the interlocking covalent bonds between its constituent carbon atoms. The interatomic spacing in diamond is 1.5445 Å, and the bond angles are all 109° as shown in Fig. 2b. Since all the valence electrons in diamond are involved in the formation of σ-bonds, diamond has very poor electrical conductivity.

## 2.3 $C_{60}$ Fullerene

The $C_{60}$ molecules, also known as the Buckminsterfullerene, were discovered in 1985 [1]. These molecules are having hollow sphere structures with 60 carbon atoms forming strong $sp^2$ covalent bonds with each other. Each $C_{60}$ molecule contains 12 pentagons and 20 hexagons, with carbon atom in each corner as shown in Fig. 3. The van der Waals diameter of a $C_{60}$ molecule is about 1 nm, while the nucleus to nucleus diameter of a $C_{60}$ molecule is about 0.7 nm. The $C_{60}$ molecule has two bond lengths, corresponding to the hexagons and pentagons. Its average bond length is 1.4 Å.

## 2.4 Carbon Nanotubes

The structure of CNTs was revealed in 1991 [2]. CNTs are seamless one-dimensional cylindrical rolls of graphene sheets. Single-wall carbon nanotubes (SWCNTs) are referring to such cylindrical molecules with single layer of graphene sheet. Multiwalled carbon nanotubes (MWCNTs) are coaxial rolls of multiple graphene sheets. MWCNTs were detected in 1991, and SWCNTs were identified two years later [12, 13]. SWCNTs were then found to have the bundling tendency due to the van der Waal forces between nanotubes [14]. Although CNTs are constructed by the conducting graphene sheets, they can be either semimetallic or semiconducting,

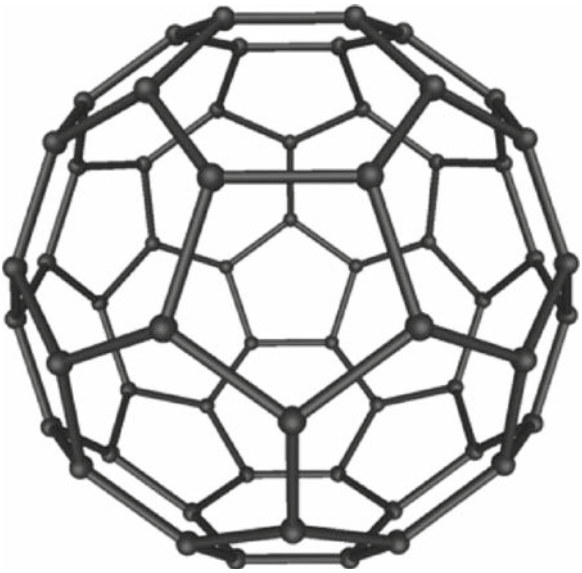

**Fig. 3** Structure of a $C_{60}$ molecule. This is a file from the Wikimedia Commons

depending upon their structures [15–19]. The typical diameter for SWCNTs is ~1.4 nm. However, CNTs with a diameter of 0.4 nm have also been reported [20].

Quantitatively, the structure of a SWCNT can be expressed in terms of a unit cell [15] defined by the chiral vector $\boldsymbol{C}_h = n\boldsymbol{a}_1 + m\boldsymbol{a}_2$. In this case, $\boldsymbol{a}_1$ and $\boldsymbol{a}_2$ are unit vectors, and $n$ and $m$ are integers often written as ($n$, $m$) to represent the chirality of a SWCNTs as shown in Fig. 4. The magnitude of the circumference is thus given by $|C_h| = a\,(n^2 + m^2 + nm)^{1/2}$, where "$a$" is the length of the unit vectors and is equal to 2.46 Å. For example, on the one hand, SWCNT (10, 0) can be constructed by folding the graphene sheet in Fig. 4 along the direction of $\boldsymbol{a}_1$ so that (0, 0) and (10, 0) will join together. In this case, $\boldsymbol{C}_h$ is parallel to $\boldsymbol{a}_1$ and forming a zero chiral angle ($\theta = 0°$). This type of SWCNTs is called zigzag nanotubes, where ($n$, 0). On the other hand, SWCNT (6, 6) can be formed by folding the graphene sheet so that (0, 0) and (6, 6) will join together. In this case, the chiral angle $\theta = 30°$. This type of SWCNTs is called armchair nanotubes and can be represented by ($n$, $n$). SWCNTs with $0° < \theta < 30°$ are called chiral nanotubes, for example SWCNT (7, 5). For all cases, the diameter of a SWCNT is given by

$$d_t = \frac{C_h}{\pi} = \frac{a(n^2 + m^2 + nm)^{1/2}}{\pi} \text{ and}$$

$$\theta = \sin^{-1}\left(\frac{m\sqrt{3}}{2n+m}\right).$$

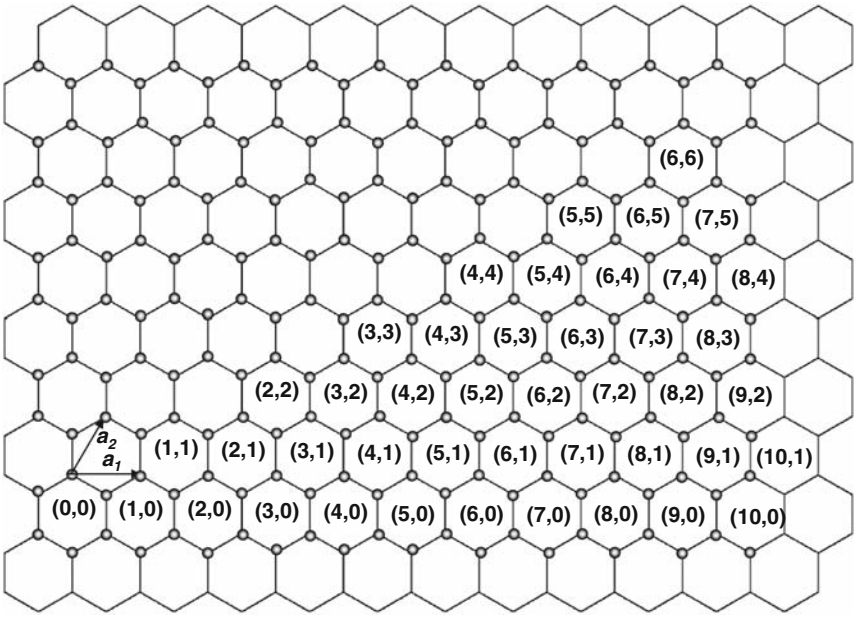


**Fig. 4** Vector ($n$, $m$) of SWCNTs on a graphene sheet

Figure 5 illustrates the appearances of (10, 0), (6, 6), and (7, 5) of SWCNTs. It was found that all armchair tubes are semimetallic like graphite. One third (1/3) of zigzag and chiral tubes are semimetallic (when $n - m = 3p$, $p$= integer) otherwise are semiconducting. As for the case of MWCNTs, they are always semimetallic, irrespective of their diameters and chiralities.

The synthesis techniques for CNTs have been widely investigated. These techniques include arc discharge [2], laser ablation [21], and chemical vapor deposition (CVD). Currently, the most well receiving technique is CVD, which was evolved from the high-temperature approaches (~1,000–1,200°C) using $CH_4$ [22, 23] or CO [24] feedstocks to the recent low temperature approaches (600-800°C). The low temperature approaches prevented aggregation of catalyst nanoparticles and have lead to high-density vertically-aligned grow mode, which requires high density of active catalyst [25, 26]. There are various low-temperature approaches including the use of water vapors [27], oxygen plasma [28], and ethanol [29]. The authors have shown that vertically-aligned single and double-walled CNTs can be grown using $C_2H_2$ source gas without the need of water, plasma, or ethanol as shown in Fig. 6 [30]. This success was obtained by controlling dissociative adsorption of $C_2H_2$ molecules by low flow rates and carrier gases [25, 26].

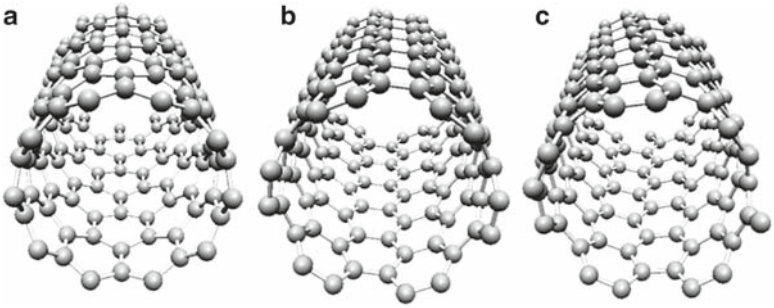


**Fig. 5** (**a**) Zigzag (10, 0), (**b**) Armchair (6, 6), and (**c**) Chiral (7, 5) CNTs

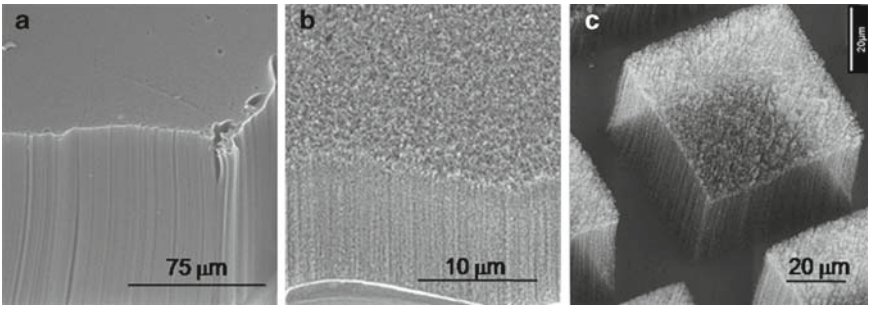


**Fig. 6** Vertically-aligned (**a**) single, (**b**) double, and (**c**) multiwalled CNTs

As discussed SWCNTs can be semimetallic or semiconducting with various band gaps depending on their chiralities. Thus it is important to characterize their chiralities prior to device fabrication. Raman spectroscopy can be used to estimate the diameters of SWCNTs from the radial breathing mode (RBM) but not the exact (*n, m*). Spectrofluorometry is a powerful tool for identifying the chirality [31]. For spectrofluorometry analysis, a well-dispersed aqueous solution of SWCNTs is prepared, and a light with certain excitation wavelength is incident on the solution. The semiconducting SWNTs undergo absorption and emission transitions, as shown in the Fig. 7a. Since certain fluorescence wavelengths will be emitted with

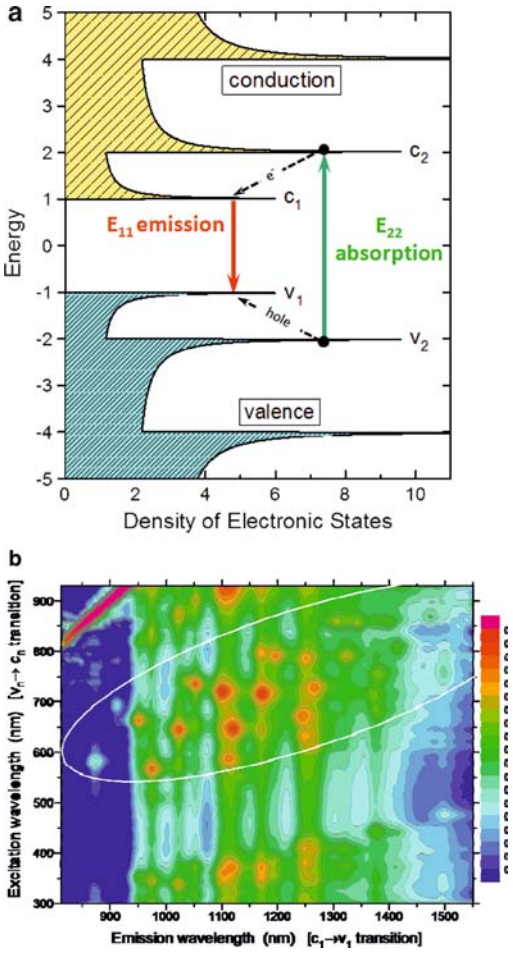


**Fig. 7** (**a**) Schematic density of electronic states for a single nanotube structure. *Solid arrows* representing the optical excitation and emission transitions. *Dashed arrows* denote nonradiative relaxation of the electron (in the conduction band) and hole (in the valence band) before emission. (**b**) Contour plot of fluorescence intensity vs. excitation and emission wavelengths for a sample of SWNTs. (Courtesy of R. B. Weisman, Original figure from [31]. Reprinted with permission from AAAS)

particular wavelength of excitation light, the chiral indices (*n, m*) can be obtained by referring to the density of states (DOS) of particular SWCNTs. The relation of the excitation and emission wavelengths can be plotted as a fluorescence contour plot as shown in Fig. 7b. The relative intensity of the spectral peaks reveals the relative quantity of each type of semiconducting SWCNTs. However, spectrofluorometry cannot identify the chirality of the semimetallic SWCNTs as they do not produce any fluorescence.

## 3 Boron Nitride

BN is constructed by boron (B) and nitrogen (N) atoms, the group III and V elements next to the group IV carbon (C) in the *Periodic Table of Elements.* Since B–N bonds and C–C bonds are isoelectronic (having the same number of electrons), BN materials are expected to form similar covalent structures to the carbon allotropes. The electronic configuration of ground state B and N atoms and hybridized B–N bonds are shown as follows:

$$\mathrm{B}\ \underset{1s}{\uparrow\downarrow}\ \underset{2s}{\uparrow\downarrow}\ \underset{2p_x}{\uparrow}\ \underset{2p_y}{\ }\ \underset{2p_z}{\ },\ \mathrm{N}\ \underset{1s}{\uparrow\downarrow}\ \underset{2s}{\uparrow\downarrow}\ \underset{2p_x}{\uparrow}\ \underset{2p_y}{\uparrow}\ \underset{2p_z}{\uparrow}$$

$$\text{for } sp^2 \rightarrow \mathrm{B}^*\ \underset{1s}{\uparrow\downarrow}\ \underset{sp^2}{\uparrow}\ \underset{sp^2}{\uparrow}\ \underset{sp^2}{\uparrow}\ \underset{2p_z}{\ },\ \mathrm{N}^*\ \underset{1s}{\uparrow\downarrow}\ \underset{sp^2}{\uparrow\downarrow}\ \underset{sp^2}{\uparrow}\ \underset{sp^2}{\uparrow}\ \underset{2p_z}{\uparrow}$$

$$\text{for } sp^3 \rightarrow \mathrm{B}^*\ \underset{1s}{\uparrow\downarrow}\ \underset{sp^3}{\uparrow}\ \underset{sp^3}{\uparrow}\ \underset{sp^3}{\uparrow}\ \underset{sp^3}{\ },\ \mathrm{N}^*\ \underset{1s}{\uparrow\downarrow}\ \underset{sp^3}{\uparrow\downarrow}\ \underset{sp^3}{\uparrow}\ \underset{sp^3}{\uparrow}\ \underset{sp^3}{\uparrow}$$

For both $sp^2$ and $sp^3$ cases, one can observe that an additional electron is localized at the nitrogen atoms. Although all the electrons in the hybridized orbitals will redistribute to form the desired bonds, these covalent bonds are having some ionic nature, more electronegative at the nitrogen site. In fact, BN can appear in *hexagonal* phase (*h*-BN), *cubic* phase (*c*-BN), *rhombohedral* phase (*r*-BN), and *wurtzite* phase (*w*-BN) as shown in Fig. 8 [32]. These phases are similar to *hexagonal* graphite (*ABAB.*), *cubic* diamonds, *rhombohedral* graphite (*ABCABC…*), and *hexagonal* diamonds (*Lonsdaleite*).

### *3.1 Phases of Boron Nitride Crystals*

*h*-BN are constructed by layers of hexagonal BN networks with lattice constants ($a_0$ = 2.504 Å, $c_0$ = 6.661 Å) comparable to those of graphite ($a_0$ = 2.458 Å, $c_0$ = 6.696 Å)

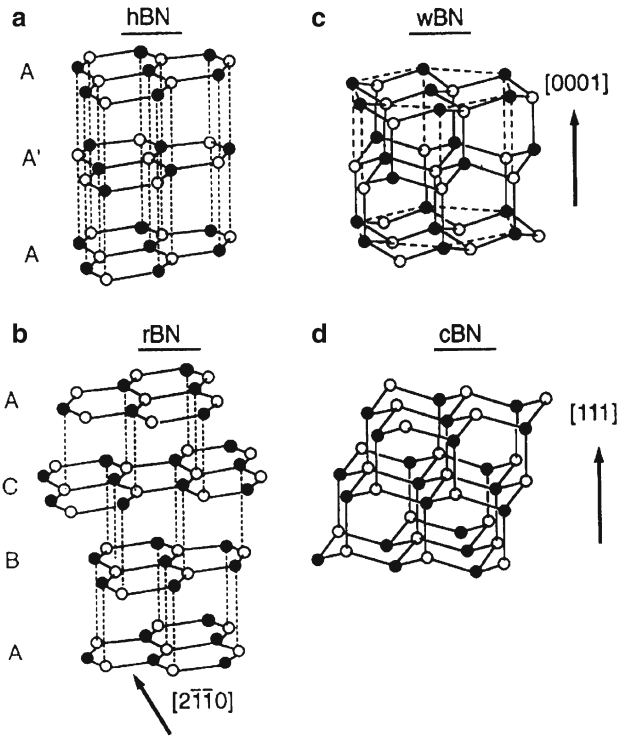


**Fig. 8** Graphical representations of (**a**) h-BN, (**b**) r-BN, (**c**) w-BN, and (**d**) c-BN phases. (From [32], Reprinted with permission from American Physical Society)

[33, Original data in 1952]. These *h*-BN layers are arranged on top of each other in an *AA'AA'*…. sequence, such that B atoms in one layer are bonded to N atoms in the adjacent layer by electrostatic interaction as shown in Fig. 8a. *Rhombohedral* phase-BN (*r*-BN) is different from *h*-BN mainly in the aspect of stacking sequence as shown in Fig. 8b [34]. The stacking sequence of *r*-BN is threefold (*ABCABC*…), and hexagonal BN rings are not perfectly overlapped with those in adjacent BN layers.

Both *wurtzite* phase-BN (*w*-BN) and *c*-BN belong to $sp^3$-bonded phases. *w*-BN is arranged in a hexagonal unit cell with puckered layers of hexagonal networks as shown in Fig. 8c [35]. The interplanar gap is much smaller than $sp^2$ phases such as *h*-BN and *r*-BN. *c*-BN [36, 37], another $sp^3$-bonded phase, possesses the *Zinc Blende* structure as shown in Fig. 8d. It consists of tetrahedrally-bonded boron and nitrogen atoms with their {111} planes settled in a trilayer (*ABCABC*…) stacking sequence. The structural parameters of the four BN phases are summarized in Table 2 [38] In addition to these four BN phases, another form of BN is called *turbostatic* phase-BN (*t*-BN) [39], which can be considered as a disordered *h*-BN or *r*-BN phase.

**Table 2** Structural properties of four boron nitride phases

| Phase | Hybridization | $a$ (Å) | $b$ (Å) | Space group | Stacking sequence |
|---|---|---|---|---|---|
| $h$-BN | $Sp^2$ | 2.5043 | 6.6562 | $P6_3/mmc$ (194) | $AA'AA'\ldots$ |
| $c$-BN | $Sp^3$ | 3.6153 | | $F43m$ (216) | $ABCABC\ldots$ |
| $r$-BN | $Sp^2$ | 2.5042 | 9.99 | $R3m$ (160) | $ABCABC\ldots$ |
| $w$-BN | $Sp^3$ | 2.5505 | 4.21 | $P6_3mc$ (186) | $AA'AA'\ldots$ |

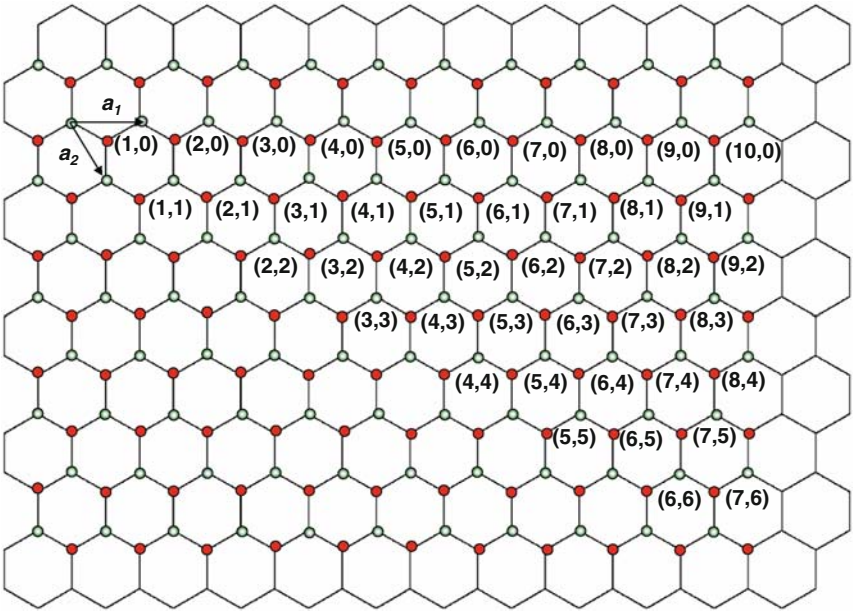


**Fig. 9** Vector ($n$, $m$) of SWBNNTs on a $h$-BN sheet

## 3.2 Boron Nitride Nanotubes

Seamless nanocylindrical rolls of $h$-BN sheets can be formed and are called BNNTs [40, 41]. Depending on the number of $h$-BN sheet involved, BNNTs can be single-walled (SW) with only single layer of $h$-BN sheet, or multi-walled (MW) that are constructed by several concentric $h$-BN sheets. An important difference between BNNTs and CNTs is that the band gap of BNNTs (~5 eV, theoretically) is insensitive to their chirality, number of walls, and diameters. As shown in Fig. 9, the chirality of SWBNNTs can be assigned in identical way as for SWCNTs. The convention of the unit vectors in this figure is chosen in the way consistent to that to be discussed in the chapter by Blasé and Chacham of this book. Again, ($n$, $m$) integers are assigned to represent the structures of SWBNNTs. SWBNNTs ($n$, 0) are zig-zag nanotubes, SWBNNTs ($n$, $n$) are armchair nanotubes, and others are chiral nanotubes.

As examples, the atomic arrangements of (a) zigzag (*10,0*), (b) armchair (*6,6*), and (c) chiral (*7,5*) SWBNNTs are illustrated in Fig. 10. Images of SWBNNTs, double-walled BNNTs, and MWBNNTs as detected by transmission electron microscopy are shown in Fig. 11 [42]. Further readings on BNNTs and related nanostructures are available in the chapters by Wang et al., Arenal and Loiseau, Blasé and Chacham, Wirtz and Rubio, and Oku et al.

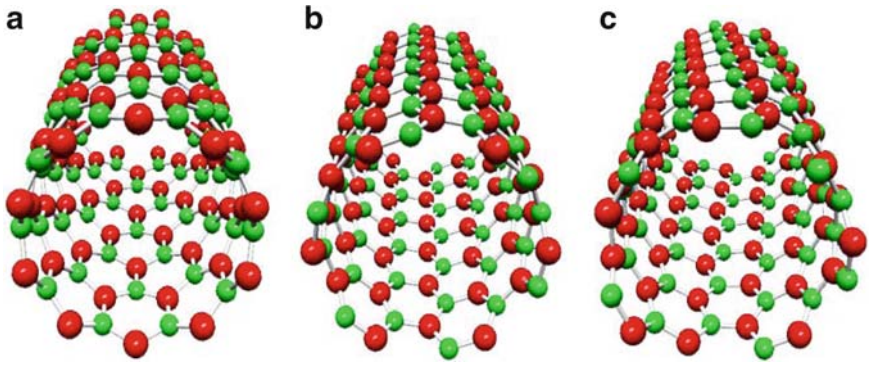


**Fig. 10** (**a**) Zigzag (10, 0), (**b**) Armchair (6, 6), (**c**) Chiral (7, 5) BNNTs

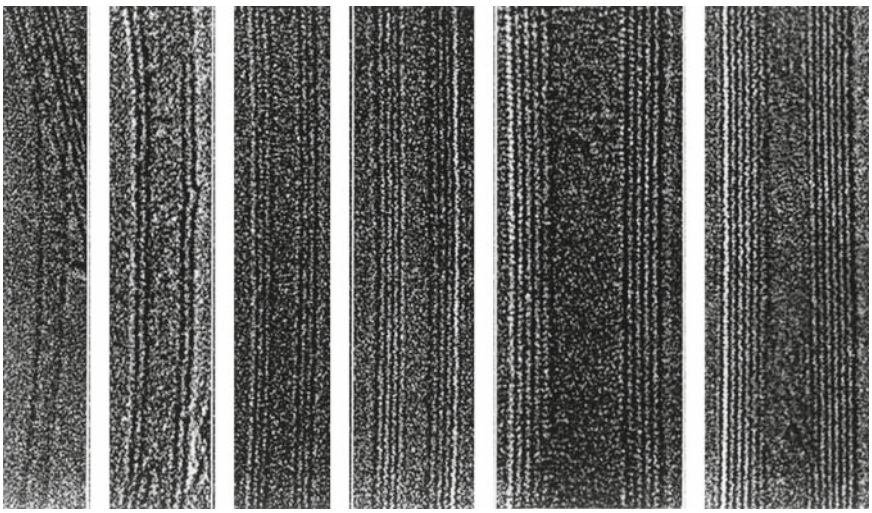

**Fig. 11** Images of transmission electron microscopy of single, to six-walled boron nitride nanotubes (*left* to *right*). (Courtesy of A. Zettl, Original figure from [42]. Reprinted with permission from American Institute of Physics)

## 4 Boron Carbide

Boron carbide ($B_4C$) is one of the hardest materials known, ranking third behind diamond and *c*-BN described earlier. In fact, ceramic of $B_4C$ are commercially produced for various applications including those in tank armor and bulletproof vests. The crystal structure of boron carbide has been known to be the rhombohedral unit cell ($B_{12}C_3$), which is composed of the closed-shell $B_{11}C$ icosahedral subunit clusters as schematically shown in Fig. 12. This unique structure is usually interpreted as follows. There are eight distorted $B_{11}C$ icosahedra located at the corners of the rhombohedral Bravais lattice. These icosahedra are connected by an atomic linear C–B–C chain within the lattice. However, the locations of the carbon atoms in the icosahedron as well as the composition (not exactly $B_{11}C$ but $B_{12-n}C_n$) are still debating. In fact, the stability of these boron carbide icosahedra in comparison to the pure boron clusters is still an active research topic [43]. In addition to $B_4C$, there have been some interesting investigations on zero, one, and two-dimensional boron carbide nanostructures. These will be discussed further in the chapter by Lau et al.

## 5 Boron

Boron is the smallest and lightest atom that can form solids with high-strength covalent bonds. In fact, β-*rhombohedral boron* is the hardest elementary crystal after diamonds. In addition, boron solids have a series of impressive properties [44]. All forms of boron (allotropes) have very high melting points, from 2,200 to 2,300°C (4,000–4,200°F). They are not reactive to oxygen, water, acids, and alkalis, and thus have high resistance to chemical attacks. Boron can appear in various forms and structures, from amorphous and crystalline phases to nanos-

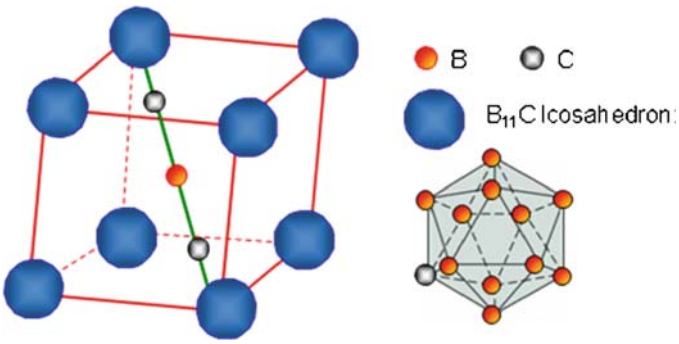


**Fig. 12** Unit cell of $B_4C$ crystals

tructures including clusters and nanotubes. Irregular bonding between boron atoms forms amorphous structures and is brown in color. Crystalline phases, however, is in black color and consists of three known structures: *α-rhombohedra* [45], *β-rhombohedral* [45], and *tetragonal* [46]. The physical and chemical properties of boron solids are expected to be enhanced by forming boron nanotubes (BNTs), boron clusters, and boron fullerenes. These closed-shell nanostructures will eliminate dangling bonds at the surface and thus avoid uncontrollable chemical reactions. In fact, the $B_{12}$*icosahedral* unit is well known as the building blocks for all the known boron polymorphs, including the *β-rhombohedral boron*. Detailed description of these boron nanostructures is available in the chapter by Lau et al. of this book.

## 6 Carbon Nitride

The research on carbon nitride had started to gain tremendous attention after the prediction of β-$C_3N_4$ in 1989 [47, 48]. According to the ab initio calculation, β-$C_3N_4$ resembled identical crystal structure as β-$Si_3N_4$ with the carbon atoms substituting the silicon atoms as shown in Fig. 13. The calculated cohesive energy of β-$C_3N_4$ suggested for a metastable carbon nitride compound. More importantly, due to their strong covalent bond, the calculated bulk modulus (4.27 Mbar) was comparable to that of diamond (4.43 Mbar). In addition to β-$C_3N_4$, other phases of $C_3N_4$ were also theoretically predicted including α-$C_3N_4$, cubic-$C_3N_4$, pseudocubic-$C_3N_4$, and graphitic-$C_3N_4$ [49].

There have been many experimental attempts in the synthesis of β-$C_3N_4$ but it was generally accepted that β-$C_3N_4$ may not be realistic materials. The synthesis of β-$C_3N_4$ was attempted by pulse laser deposition in 1993 [50]. Although crystalline structure was claimed, the nitrogen contents in these films was only approximately

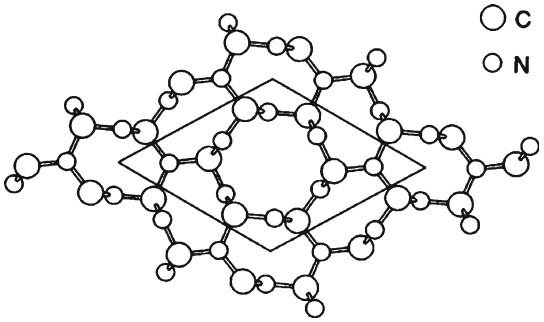


**Fig. 13** Structure of β-$C_3N_4$ in the *a*–*b* plane. The *c*-axis is normal to the page. Half the atoms illustrated are located in the $z = -c/4$ plane, the other half are in the $z = c/4$ plane. The structure consists of these buckled planes stacked in *AAA*… sequence. The parallelogram shows the unit cell. (From [47], Reprinted with permission from AAAS)

45%, which was less than that predicted for the $C_3N_4$ stoichiometry (57%). In the later experiments [51–53], it was found that the carbon atoms in the carbon nitride thin film were transformed from the initial $sp^3$ hybridization to $sp^2$-bonded carbon when the overall nitrogen contents increased. The density of the film was decreased from 3.3 to 2.1 g/cm$^3$ when the concentration of nitrogen increased from 11-17%. Many other techniques have been used for the synthesis of carbon nitride films including arc discharge [54], RF plasma enhanced pulsed-laser deposition [55–58], RF sputtering [59–63], hot filament plasma sputtering [64], magnetron sputtering [65–69], plasma enhanced CVD (PECVD) [70–73], ion beam sputtering [74–78], other ion or reactive atom beam deposition techniques [79–82], and atmospheric pressure plasma [83]. Most of these attempts were conducted at room temperature, merely the doping of nitrogen into the $sp^3$ hybridization amorphous diamond-like carbon matrix. High temperature attempt was shown to reverse the $sp^2$C=N bonds into $sp^3$C-N bonds needed for β-$C_3N_4$ [55–57]. However, the nitrogen contents were below 16 at.%.

Although the attempts in growing for $C_3N_4$ were not succeeded, nanoscale $CN_x$ particles or films were found to be promising to be a hard material [84]. Similar to the thin film studies, PECVD [85], plasma sputtering deposition [86], and chemical reaction [87] had been utilized to produce the CN nanoparticles. Apparently, nanoscale carbon nitride compounds appear to be the important area in the future, including the nitrogen-doped CNTs and nanostructures to be discussed in the chapters by Arenal and Loiseau, Yu and Wang, and Filho and Terrones of this book.

## 7 Boron Carbon-Nitride

Since carbon and BN phases are structurally similar, many efforts have been invested in exploring their hybrid phases. These attempts can be classified into three: (1) hexagonal phase boron carbon-nitride ($h$-$B_xC_yN_z$) that could have intermediate properties between those of graphite and $h$-BN, (2) cubic phase boron carbon-nitride ($c$-$B_xC_yN_z$) that will be superhard like diamonds and $c$-BN, and (3) nanohybrids that may have intermediate or modified properties between those of CNTs and BNNTs.

The efforts of producing $h$-$B_xC_yN_z$ and $c$-$B_xC_yN_z$ bulks and thin films have been initiated since 1980s [88-92], and extended into 1990s [93-100]. In fact, the first report on hybridized $B_xC_yN_z$ compounds was having grain dimension below 20 nm [88]. These results indicate that $B_xC_yN_z$ compounds should be considered as nanstructures or nanocrystals instead of macroscopic single crystals as suggested in recent review articles [101, 102]. In fact, the research interest on $B_xC_yN_z$ hybrids appears to move toward $B_xC_yN_z$ nanotubes and nanostructures, after the demonstration of CNTs and BNNTs.

### *7.1 Hexagonal Phase Hybrid: h-$B_xC_yN_z$*

As discussed, graphite is semimetallic and $h$-BN is insulating with a wide band gap ≥5.8 eV [103, 104]. Since graphite and $h$-BN are constructed by layers of carbon and BN honeycombs, respectively, it was anticipated that new $h$-$B_xC_yN_z$ hybrid

**Table 3** Bond lengths of various types of bonds in h-$BC_2N$ hybrids [105, 106]

| Bonds | Bond lengths/nm |
|---|---|
| C-C | 0.142 |
| B-C | 0.155 |
| B-N | 0.145 |
| C-N | 0.132 |

These data are also applicable for $BC_2N$ nanotubes

phase would have BCN honeycomb structures. These *h*-$B_xC_yN_z$ hybrids may have energy band gap smaller than that of *h*-BN, a new semiconducting materials. Theory on *h*-$BC_2N$ sheets was then proposed, which consist of various chemical bonds as shown in Table 3.

The attempt of producing *h*-$B_xC_yN_z$ was motivated by their attractive physical properties such as controllable band gap by varying their composition and chemical inertness. For example, recent attempts on growing $B_xC_yN_z$ thin films have involved various approaches including CVD [107, 108], ion beam assisted deposition [109], magnetron sputtering [110, 111], RF plasma enhanced pulsed-laser deposition [112, 113], excimer laser annealing [114], and arc discharge [115]. However, most of these thin films are amorphous phase. In fact, the most challenging obstacle for producing crystalline *h*-$B_xC_yN_z$ bulks and thin films is phase separation. Most $B_xC_yN_z$ compounds are mixtures of pure BN and graphite domains. Recent results shown that hybridized *h*-$B_xC_yN_z$ compounds tend to stabilize in nanostructures [116].

## *7.2 Cubic Phase Hybrid: c-$B_xC_yN_z$*

The major motivation for the search of cubic phase $B_xC_yN_z$ (*c*-$B_xC_yN_z$) compounds is to realize new superhard materials that may be harder than *c*-BN. Although *c*-BN is the second hardest known materials, it has only half the hardness of diamonds. Furthermore, the synthesis of *c*-BN crystals and thin films is much harder than those of diamonds. However, *c*-BN is chemically inert to ferrous metals and more stable than diamond at high temperatures in the presence of oxygen. It was believed that *c*-$BC_2N$ could be harder than *c*-BN and chemically stable like *c*-BN. Various *c*-$BC_2N$ structures have been studied by the ab initio pseudopotential density functional method, based on the eight-atom Zinc Blende structured cubic unit cell [117]. All the structures are having positive total energy indicating of their metastable nature. Thus *c*-$B_xC_yN_z$ is expected to be formed under high pressure and high temperature (HPHT) condition.

In fact, the growth of *c*-$B_xC_yN_z$ hybrid was reported in 1981. This was carried out in a diamond anvil cell at a static pressure of 14 GPa and a temperature of 3,000°C [118]. Polycrystalline *h*-$B_xC_yN_z$ powders [88] produced by CVD were used

as the starting materials without any catalyst (which is needed for the growth of *c*-BN and diamonds). The composition of the products was $(BN)_{0.26}C_{0.74}$, similar to that of the starting materials. These *c*-$(BN)_{0.26}C_{0.74}$ hybrids had lattice constant of 0.3582 ± 0.0002 nm, in between that of diamond (0.3570 ± 0.0001 nm) and *c*-BN (0.3615 ± 0.0001 nm). These hybrids were polycrystals, with dimensions of several micrometers. However, transmission electron microscopy (TEM) indicates that the grain size of these cubic hybrids is on the order of nanometers [101]. Similar experiments were then conducted by using a laser-heated diamond cell [119]. The lattice constants of the products [*c*-$B_{0.35}C_{0.3}N_{0.35}$ and *c*-$B_{0.2}C_{0.6}N_{0.2}$] were 0.3613 ± 0.0003 nm and 0.3596 ± 0.0003 nm, respectively. The bulk modulus of *c*-$B_{0.33}C_{0.33}N_{0.33}$ was determined as 355 ± 19 GPa, lower than those of diamond (442 GPa) and c-BN (369 GPa).

There was also an attempt to transform *h*-$B_xC_yN_z$ to *c*-$B_xC_yN_z$ hybrids at HPHT condition using catalyst. Cobalt (Co) was used in these experiments, which were conducted at a pressure of 5.5 GPa and temperature of 1,400-1,600°C [120]. Later experiment was carried out without using any catalyst at 7.7 GPa and 2,000–2,400°C [121, 122]. However, the *c*-$B_xC_yN_z$ product was phase separated into *c*-BCN and diamonds at high temperature. The cubic phase crystals were typically 20-30 nm in diameter. Recently, *c*-$BC_2N$ was synthesized from graphite-like $BC_2N$ at pressures above 18 GPa and temperatures higher than 2,200 K [123]. The hardness of *c*-$BC_2N$ is higher than that of *c*-BN and slightly less hard than diamond. This is the low-density *c*-BCN structure proposed by the recent theoretical modeling [124].

In addition to the HPHT techniques, other methods such as reactive vapor phase deposition [125] and ball milling [126, 127] have been attempted to synthesize *c*-$B_xC_yN_z$ hybrids. In general, the *c*-$B_xC_yN_z$ tends to phase separate into *c*-BN and diamonds.

## 7.3 $B_xC_yN_z$ Nanostructures

Since 1994, $BC_2N$ nanotubes have been studied theoretically [128] and experimentally [129–131]. Unlike pure CNTs, the electronic structure of $B_xC_yN_z$ nanotubes is predicted to be prominently influenced by their chemical composition, rather than their geometrical structure [132]. Theoretically, the energy bandgap of $B_xC_yN_z$ nanotubes are tunable by varying their atomic compositions. They may have potential applications in photoluminescence and photonics applications, as well as nanoelectronic devices or sensors working at high temperature.

In addition to the earlier attempts in growing $B_xC_yN_z$ nanotubes by arc discharge and laser ablation [129–131], an interesting technique called substitution reaction was also demonstrated. This technique was initially invented to produce BNNTs [133–135]. In short, CNTs was used as the templates and reacted with $B_2O_3$ powder in the presence of $N_2$ gas at 1,600°C to form $B_xC_yN_z$ nanotubes. Further thermal oxidation heating of these products in air at 700°C would convert the $B_xC_yN_z$ nanotubes into BNNTs with an efficiency of 60%. Later, this substitution method was modified by adding metal oxide promoters in the reaction for the growth of both $B_xC_yN_z$

nanotubes and BNNTs [136–138]. Results indicate that these $B_xC_yN_z$ nanotubes were radially phase-separated into BN and carbon shells [139] The carbon shells formed in the outer or inner layers of the multiwalled structure, rather than being sandwiched between BN shells.

Recently, a significant advancement had been reported to directly synthesize single wall $B_xC_yN_z$ nanotubes by using bias-assisted hot filament CVD method [140, 141]. In brief, $CH_4$, $B_2H_6$, and ethylenediamine vapor were flowed to the growth chamber as the reactant gases. MgO-supported Fe-Mo bimetallic powders were used as the catalyst. The boron and nitrogen contents of these nanotubes are still low. The chapters by Arenal and Loiseau, Blasé and Chacham, and Yu and Wang are devoted to describe current research status on $B_xC_yN_z$ nanostructures. Readers are encouraged to find more information in previous reviews on $B_xC_yN_z$ nanostructures [101, 102, 142].

## 8 Doped CNTs

Since the discovery of CNTs, quasi one-dimensional material has become the research of interest. It has been shown theoretically that CNTs doped with exotic elements may alter the band structure and morphological properties of CNTs [143]. There have been some experimental works on boron-doped CNTs [144, 145] and nitrogen-doped CNTs [146, 147] have been demonstrated. For example, nitrogen-doping was shown to enhance electron field emission properties of multiwalled CNTs [148]. The chapter by Filho and Terrones highlights the research on doped CNTs.

**Acknowledgment** Y. K. Yap acknowledges National Science Foundation CAREER Award (DMR 0447555) for supporting the project on frontier carbon materials; the U.S. Department of Energy, Office of Basic Energy Sciences (DE-FG02-06ER46294) for in part supporting the project on boron nitride nanotubes; and the U.S. Department of Army (W911NF-04-1-0029) and the Defense Advanced Research Projects Agency (DAAD17-03-C-0115 through Army Research Laboratory) for supporting his projects on CNTs.

## References

1. H. W. Kroto, J. R. Heath, S. C. O'Brien, R. F. Curl, and R. E. Smalley, Nature (London) **318**, 162 (1985).
2. S. Iijima, Nature (London) **354**, 56 (1991).
3. http://nobelprize.org/nobel_prizes/chemistry/laureates/1996/
4. T. W. Capehart, T. A. Perry, C. B. Beetz, D. N. Belton, G. B. Fisher, C. E. Beall, B. N. Yates, and J. W. Taylor, Appl. Phys. Lett. **55**, 957 (1989).
5. R. Saito, G. Dresselhaus, and M. S. Dresselhaus, Physical Properties of Carbon nanotubes, Imperial College Press, London (1998).
6. M. S. Dresselhaus and G. Dresselhaus, Eds., Carbon Nanotubes: Synthesis, Structure, Properties and Applications, Springer-Verlag, Berlin (2001).
7. M. W. Geis and M. A. Tamor, in Encyclopedia of Applied Physics, Vol. 5, Diamond and Diamond-like Carbon, G. L. Trigg, Eds., VCH Publishers, Inc., New York, 1–24 (1993).

8. O. J. Vohler, F. von Sturm, and E. Wege, in Encyclopedia of Applied Physics, Vol. 3, Carbon Materials, G. L. Trigg, Eds., VCH Publishers, Inc., New York, 21–40 (1993).
9. M. S. Dresselhaus and G. Dresselhaus, in Encyclopedia of Applied Physics, Vol. 7, Graphite, G. L. Trigg, Eds., VCH Publishers, Inc., New York, 289–301 (1993).
10. A. Y. Liu, R. M. Wentzcovitch, and M. L. Cohen, Phys. Rev. B **39**, 1760 (1989).
11. http://www.nsf.gov/awardsearch/showAward.do?AwardNumber=0447555. Y. K. Yap, National Science Foundation Award # 0447555, "CAREER: Synthesis, Characterization and Discovery of Frontier Carbon Materials.
12. S. Iijima and T. Ichihashi, Nature (London) **363**, 603 (1993).
13. D. S. Bethune, C. H. Kiang, M. S. de Vries, G. Gorman, R. Savoy, J. Vazquez, and R. Beyers, Nature (London) 363, 605 (1993).
14. A. Thess, R. Lee, P. Nikolaev, H. Dai, P. Petit, J. Robert, C. Xu, Y. H. Lee, S. G. Kim, A. G. Rinzler, D. T. Colbert, G. E. Scuseria, D. Tomanek, J. E. Fisher, and R. E. Smalley, Science 273, 483 (1996).
15. M. S. Dresselhaus, G. Dresselhaus, and R. Saito, Phys. Rev. B **45**, 6234 (1992).
16. J. W. Mintmire, B. I. Dunlap, and C. T. White, Phys. Rev. Lett. **68**, 631 (1992).
17. N. Hamada, S. Sawada, A. Oshiyama, Phys. Rev. Lett. **68**, 1579 (1992).
18. J. W. G. Wilder, L. C. Venema, A. G. Rinzler, R. E. Smalley, and C. Dekker, Nature (London) **391**, 59 (1998).
19. T. W. Odom, J. L Huang, P. Kim, and C. M. Lieber, Nature (London) **391**, 62 (1998).
20. N. Wang, Z. K. Tang, G. D. Li, and J. S. Chen, Nature **408**, 50 (2000).
21. T. Guo, P. Nikolaev, A. G. Rinzler, D. Tomanek, D. T. Colbert, and R. E. Smalley, J. Phys. Chem. **99**, 10694 (1995).
22. A. Peigney, Ch. Laurent, F. Dobigeon, and A. Rousset, J. Mater. Res. **12**, 613 (1997).
23. J. H. Hafner, M. J. Bronikowski, B. R. Azamian, P. Nikolaev, A. G. Rinzler, D. T. Colbert, K. A. Smith, and R. E. Smalley, Chem. Phys. Lett. **296**, 195 (1998).
24. H. Dai, A. G. Rinzler, P. Nikolaev, A. Thess, D. T. Colbert, and R. E. Smalley, Chem. Phys. Lett. **260**, 471 (1996).
25. V. Kayastha, Y. K. Yap, S. Dimovski, and Y. Gogotsi, Appl. Phys. Lett. **85**, 3265 (2004).
26. V. Kayastha, Y. K. Yap, Z. Pan, I. N. Ivanov, A. A. Puretzky, and D. B. Geohegan, Appl. Phys. Lett. **86**, 253105 (2005).
27. K. Hata, D. N. Futaba, K. Mizuno, T. Namai, M. Yumura, and S. Iijima, Science **306**, 1362 (2004).
28. G. Zhang, D. Mann, L. Zhang, A. Javey, Y. Li, E. Yenilmez, Q. Wang, J. P. McVittie, O. Nishi, J. Gibbons, and H. Dai, PNAS **102**, 16141 (2005).
29. Y. Murakami, S. Chiashi, Y. Miyauchi, M. Hu, M. Ogura, T. Okubo, and S. Maruyama, Chem. Phys. Lett. **385**, 298 (2004).
30. V. K. Kayastha, S. Wu, J. Moscatello, and Y. K. Yap, J. Phys. Chem. C **111**, 10158 (2007).
31. S. M. Bachilo, M. S. Strano, C. Kittrell, R. H. Hauge, R. E. Smalley, and R. B. Weisman, Science **298**, 2361 (2002).
32. D. L. Medlin, T. A. Friedmann, P. B. Mirkarimi, M. J. Mills, and K. F. McCarty, Phys. Rev. B. **50**, 7884 (1994).
33. R. S. Pease, Acta. Cryst. **5**, 356 (1952).
34. T. Ishii, T. Sato, Y. Sekikawa, and M. Iwata, J. Cryst. Growth **52**, 285 (1981)
35. F. P. Bundy and R. H. Wentorf, Jr, J. Chem Phys. **38**, 1144 (1963)
36. R. H. Wentorf, Jr., J. Chem. Phys. **34**, 809 (1961)
37. C. B. Samantaray and R. N. Singh, Int. Mater. Rev., **50**, 313 (2005)
38. P. B. Mirkarimi, K. F. McCarty, and D. L. Medlin, Mat. Sci. Eng. R **21**, 47 (1997)
39. J. Thomas,N. E. Weston, and T. E. O'Connor, J. Am. Chem. Soc. **84**, 4619 (1963)
40. A. Rubio, J. L. Corkill, and M. L. Cohen, Phys. Rev. B. **49**, 5081 (1994).
41. X. Blase, A. Rubio, S. G. Louie, and M. L. Cohen, Euro. Phy. Lett. **28**, 335 (1994)
42. M. Ishigami, S. Aloni and A. Zettl, AIP Conf. Proc. **696**, 94 (2003).
43. D. Ghosh, G. Subhash, C. H. Lee, Y. K. Yap, Appl. Phys. Letts. **91**, 061910 (2007).

44. R. Naslain, in Boron and Refractory Borides, V. I. Matkovich, Ed., Springer-Verlag, New York, 139 (1977).
45. G. Will and K. Ploog, Nature **251**, 406 (1974).
46. A. W. Laubengayer, D. T. Hurd, A. E. Newkirk, and J. L. Hoard, J. Am. Chem. Soc. **65**, 1924 (1943).
47. A. Y. Liu and M. L. Cohen, Science **245**, 841 (1989).
48. A. Y. Liu and M. L. Cohen, Phys. Rev. B **41**, 10727 (1990).
49. D. M. Teter and R. J. Hemley, Science **271**, 53 (1996).
50. C. M. Niu, Y. Z. Lu, and C. M. Lieber, Science **261**, 334 (1993).
51. C. M. Lieber and Z. J. Zhang, Chem. Indus. **22**, 922 (1995).
52. J. T. Hu, P. D. Yang, and C. M. Lieber, Phys. Rev. B **57**, R3185 (1998).
53. J. T. Hu, P. D. Yang, and C. M. Lieber, Appl. Surf. Sci. **127–129**, 569 (1998).
54. O. Matsumoto, T. Kotaki, H. Shikano, K. Takemura, and S. Tanaka, J. Electrochem. Soc. **141**, L16 (1994).
55. Y. K. Yap, S. Kida, T. Aoyama, Y. Mori, and T. Sasaki, Appl. Phys. Lett. **73**, 915 (1998).
56. Y. K. Yap, S. Kida, T. Aoyama, Y. Mori, and T. Sasaki, Diamond Relat. Mater. **8**, 614 (1999).
57. Y. K. Yap, S. Kida, T. Aoyama, Y. Mori, and T. Sasaki, Diamond Relat. Mater. **9**, 1228 (2000).
58. M. Itoh, Y. Suda, M. A. Bratescu, Y. Sakai, and K. Suzuki, Appl. Phys. A **79**, 1575 (2004).
59. Y. A. Li, Z. B. Zhang, S. S. Xie, and G. Z. Yang, Chem. Phys. Lett. **247**, 253 (1995).
60. Z. B. Zhang, Y. A. Li, S. S. Xie, and G. Z. Yang, J. Mater. Sci. Lett. **14**, 1742 (1995).
61. S. Kumar, K. S. A. Butcher, and T. L. Tansley, J. Vac. Sci. Technol. A **14**, 2687 (1996).
62. C. Y. Hsu and F. C. N. Hong, Jpn. J. Appl. Phys **37**, L1058 (1998).
63. W. Lu and K. Komvopoulos, J. Appl. Phys. **85**, 2642 (1999).
64. J. Peng, P. Zhang, Y. Guo, and G. H. Chen, Mater. Lett. **29**, 191 (1996).
65. Y. A. Li, S. Xu, H. S. Li, and W. Y. Luo, J. Mater. Sci. Lett. **17**, 31 (1998).
66. L. D. Jiang, A. G. Fitzgerald, and M. J. Rose, Appl. Surf. Sci. **158**, 340 (2000).
67. J. Wei, J. Appl. Phys. **89**, 4099 (2001).
68. X. C. Wang, P. Wu, Z. Q. Li, E. Y. Jiang, and H. L. Bai, J. Phys. D: Appl. Phys. **37**, 2127 (2004).
69. M. Lejeune, O. Durand-Drouhin, S. Charvet, A. Zeinert, and M. Benlahsen, J. Appl. Phys. **101**, 123501 (2007).
70. T. Y. Yen and C. P. Chou, Appl. Phys. Lett. **67**, 2801 (1995).
71. Y. F. Zhang, Z. H. Zhou, and H. L. Li, Appl. Phys. Lett. 68, 634 (1996).
72. H. K. Woo, Y. F. Zhang, S. T. Lee, C. S. Lee, Y. W. Lam, and K. W. Wong, Diamond Relat. Mater. **6**, 635 (1997).
73. J. L. He and W. L. Chang, Surf. Coat. Technol. **99**, 184 (1998).
74. J. P. Riviere, D. Texier, J. Delafond, M. Jaouen, E. L. Mathe and J. Chaumont, Mater. Lett. **22**, 115 (1995).
75. A. Fernandez, P. Prieto, C. Quiros, J. M. Sanz, J. M. Martin and B. Vacher, Appl. Phys. Lett. **69**, 764 (1996).
76. X. W. Su, H. W. Song, F. Z. Cui, W. Z. Li, and H. D. Li, Surf. Coat. Technol. **84**, 388 (1996).
77. Z. C. Wu, Y. H. Yu, and X. H. Liu, Appl. Phys. Lett. **68**, 1291 (1996).
78. X. M. He, L. Shu, W. Z. Li, and H. D. Li, J. Mater. Res. **12**, 1595 (1997).
79. J. Y. Feng, Y. Zheng, and J. Q. Xie, Mater. Lett. **27**, 219 (1996).
80. P. N. Wang, Z. Guo, X. T. Ying, J. H. Chen, X. M. Xu, and F. M. Li, Phys. Rev. B **59**, 13347 (1999).
81. Y. G. Li, A. T. S. Wee, C. H. A. Huan, W. S. Li, and J. S. Pan, Surf. Interface Anal. **28**, 221 (1999).
82. Kazuhiro Yamamoto, Jpn. J. Appl. Phys. **44**, 1879 (2005).
83. T. Hidekazu, M. Sougawa, K. Takarabe, S. Sato, and O. Ariyada, Jpn. J. Appl. Phys. **46**, 1596 (2007).
84. D. Li, X.-W. Lin, S.-C. Cheng, V. P. Dravid, Y.-W. Chung, M.-S. Wong, and W. D. Sproul, Appl. Phys. Lett. **68**, 1211 (1996).
85. J. Pereira, I. G. Grenier, and V. M. Guilbaud, Thin Solid Films **482**, 226 (2005).
86. H. Y. Li, Y. C. Shi, and P. X. Feng, Appl. Phys. Lett. **89**, 142901 (2006).

87. T. C. Mu, J. Huang, Z. M. Liu, B. X. Han, Z. H. Li, Y. Wang, T. Jiang, and H. X. Gao, J. Mater. Res. **19**, 1736 (2004).
88. A.R. Badzian et al. in "*Proceeding of the 3rd International Conference on Chemical Vapor Deposition*" (F.A. Claski, Ed.), pp. 747–753. American Nuclear Society, Hinsdale, IL, 1972.
89. K. Montasser, S. Hattori, and S. Monita, Thin Solid Films **117**, 311 (1984).
90. L. Maya, J. Am. Ceram. Soc. **71**, 1104 (1988).
91. J. Kouvetaksi, T. Sasaki, C. Shen, R. Hagiwara, M. Lerner, K. M. Krishnan, and N. Bartlett, Synth. Metals **34**, 1 (1989).
92. L. Maya and L. A. Harris, J. Am. Ceram. Soc. **73**, 1912 (1990).
93. M. Yamada, M. Nakaishi, and K. Sugishima, J. Electrochem. Soc. **137**, 2242 (1990).
94. T. M. Besmann, J. Am. Ceram. Soc. **73**, 2498 (1990).
95. M. Morita, T. Hanada, H. Tsutsumi, Y. Matsuda, and W. Kawaguchi, J. Electrochem. Soc. **139**, 1227 (1992).
96. F. Saugnac, F. Teyssandiev, and A. Marchand, J. Am. Ceram. Soc. **75**, 161 (1992).
97. N. Kawaguchi and T. Kawashima, J. Chem. Soc., Chem. Commun. **14**, 1133 (1993).
98. A. Derré, L. Filipozzi, F. Bouyer, and A. Marchand, J. Mater. Sci. **29**, 1589 (1994).
99. M. Hubacek and T. Sato, J. Solid State Chem. 114, 258 (1995).
100. M. O. Watanabe, S. Itoh, K. Mizushima, and T. Sasaki, Thin Solid Films **281-282**, 334 (1996).
101. Y. K. Yap, "Boron-Carbon Nitride Nanohybrids," in *Encyclopedia of Nanoscience and Nanotechnology* (Foreword by R. E. Smalley), H. S. Nalwa, Ed., Volume **1**, 383–394, American Scientific Publishers, (2004).
102. C. H. Lee and Y. K. Yap," Current Research Status of Boron-Carbon Nitride Bulks, Thin Films, and Nanostructures," Chapter 10, in *Diamond and Related Materials Research*, Shôta Shimizu Ed., Nova Science Publisher, New York, 277–292 (2008).
103. M. Yano, Y. K. Yap, M. Okamoto, M. Onda, M. Yoshimura, Y. Mori, and T. Sasaki, Jpn. J. Appl. Phys. **39**, L300 (2000).
104. Y. Kubota, K. Watanabe, O. Tsuda, and T. Taniguchi, Science **317**, 932 (2007).
105. Y. Miyamoto, A. Rubio, M. L. Cohen, and S. G. Louie, Phys. Rev. B **50**, 4976 (1994).
106. A. Y. Liu, R. M. Wentzcovitch, and M. L. Cohen, Phys. Rev. B **39**, 1760 (1989).
107. T. Yuki, S. Umeda, and T. Sugino, Diamond Relat. Mater. **13**, 1130 (2004).
108. J. Yu, E. G. Wang, J. Ahn, S. F. Yoon, Q. Zhang, J. Cui, and M. B. Yu, J. Appl. Phys. **87**, 4022 (2000).
109. R. Gago, I. Jiménez, and J. M. Albella, Thin Solid Films 373, 277 (2000).
110. M. K. Lei,.Quan Li, Z. F. Zhou, I. Bello, C. S. Lee, and S. T. Lee, Thin Solid Films **389**, 194 (2001).
111. D. H. Kim, E. Byon, S. Lee, J.-K. Kim, and H. Ruh, Thin Solid Films **447-448**, 192 (2004).
112. Y. Wada, Y. K. Yap, M. Yoshimura, Y. Mori, and T. Sasaki, Diamond Relat. Mater. **9**, 620 (2000).
113. Y. K. Yap, Y. Wada, M. Yamaoka, M. Yoshimura, Y. Mori, and T. Sasaki, Diamond Relat. Mater. **10**, 1137 (2000).
114. H. Aoki, K. Ohyama, H. Sota, T. Seino, C. Kimura, and T. Sugino, Appl. Surf. Sci. **254**, 596 (2007).
115. Pi-Chuen Tsai, Surf. Coat. Technol. **201**, 5108 (2007).
116. Y. K. Yap, M. Yoshimura, Y. Mori, and T. Sasaki, Appl. Phys. Lett. **80**, 2559 (2002).
117. H. Sun, S.-H. Jhi, D. Roundy, M. L. Cohen, and S. G. Louie, Phys. Rev. B **64**, 094108 (2001).
118. A. R. Badzian, Mat. Res. Bull. **16**, 1385 (1981).
119. E. Knittle, R. B. Kaner, R. Jeanloz, and M. L. Cohen, Phys. Rev. B **51**, 12149 (1995).
120. T. Sasaki, M. Akaishi, S. Yamaoka, Y. Fujiki, and T. Oikawa, Chem. Mater. **5**, 695 (1993).
121. S. Nakano, M. Akaishi, T. Sasaki, and S. Yamaoka, Chem. Mater. **6**, 2246 (1994).
122. S. Nakano, M. Akaishi, T. Sasaki, and S. Yamaoka, Mater. Sci. Eng. A **209**, 26 (1996).
123. Y. Zhao, D. W. He, L. L. Daemen, T. D. Shen, R. B. Schwarz, Y. Zhu, D. L. Bish, J. Huang, J. Zhang, G. Shen, J. Qian, and T. W. Zerda, J. Mater. Res. **17**, 3139 (2002).

124. E. Kim, T. Pang, W. Utsumi, V. L. Solozhenko, and Y. Zhao, Phys. Rev. B **75**, 184115 (2007).
125. S. Ulrich, H. Ehrhardt, T. Theel, J. Schwan, S. Westermeyr, M. Scheib, P. Becker, H. Oechsner, G. Dollinger, and A. Bergmaier, Diamond Relat. Mater. **7**, 839 (1998).
126. Yao, L. Liu and W. H. Su, J. Mater. Res. **13**, 1753 (1998).
127. J. Huang, Y. Zhu and H. Mori, J. Mater. Res. **16**, 1178 (2001).
128. Y. Miyamoto, A. Rubio, M. L. Cohen, and S. G. Louie, Phys. Rev. B **50**, 4976 (1994).
129. Z. W. Sieh, K. Cherrey, N. G. Chopra, X. Blasé, Y. Miyamoto, A. Rubio, M. L. Cohen, S. G. Louie, A. Zettl, and R. Gronsky, Phys. Rev. B **51**, 11229 (1995).
130. Y. Zhang, H. Gu, K. Suenaga, and S. Iijima, Chem. Phys. Lett. **279**, 264 (1997)
131. M. Terrones, A. M. Benito, C. Manteca-Diego, W. K. Hsu, O. I. Osman, J. P. Hare, D. G. Reid, H. Terrones, A. K. Cheetham, K. Prassides, H. W. Kroto, and D. R. M. Walton, Chem. Phys. Lett. **257**, 576 (1996).
132. X. Blasé, J.C. Charlier, A. De Vita, and R. Car, Appl. Phys. Lett. **70**, 197 (1997).
133. W. Q. Han, Y. Bando, K. Kurashima, and T. Sato, Jpn. J. Appl. Phys. **38**, L755, (1999).
134. W.-Q. Han, J. Cumings, X. Huang, K. Bradley, and A. Zettl, Chem. Phys. Lett. 346, 368 (2001).
135. W.-Q. Han, W. Mickelson, J. Cuming, and A. Zettl, Appl. Phys. Lett. 81, 1110 (2002).
136. M. Terrones, D. Golberg, N. Grobert, T. Seeger, M. R. Reyes, M. Mayne, R. Kamalakaran, P. Dorozhkin, Z.-C. Dong, H. Terrones, M. Ruhle, and Y. Bando, Adv. Mater. **15**, 1899 (2003).
137. D. Golberg, P. Dorozhkin, Y. Bando, M. Hasegawa, and Z.-C. Dong, Chem. Phys. Lett. **359**, 220 (2002).
138. D. Golberg, Y. Bando, K. Kurashima, and T. Sato, Solid State Commun. 116, 1 (2000).
139. J. Wu, W.-Q. Han, W. Walukiewicz, J. W. AgerIII, W. Shan, E. E. Haller, and A. Zettl, Nano Lett. **4**, 647 (2004).
140. C. Y. Zhi, J. D. Guo, X. D. Bai, and E. G. Wang, J. Appl. Phys. **91**, 5325 (2002).
141. W. L. Wang, X. D. Bai, K. H. Liu, Z. Xu, D. Golberg, Y. Bando, and E. G. Wang, J. Am. Chem. Soc. **128**, 6530 (2006).
142. R. Ma, D. Golberg, Y. Bando, and T. Sasaki, Phil. Trans. R. Soc. Lond. A, **362**, 2161 (2004).
143. Y. Miyamoto, M. L. Cohen, and S. G. Louie, Solid State Commun. **102**, 605 (1997).
144. W.Q. Han, Y. Bando, K. Kurashima, and T. Sato, Chem. Phys. Lett. **299**, 368 (1999).
145. L. S. Panchakarla, A. Govindaraj, and C. N. R. Rao, ACS Nano **1**, 494 (2007).
146. R. Czerw, M. Terrones, J.-C. Charlier, X. Blase, B. Foley, R. Kamalakaran, N. Grobert, H. Terrones, D. Tekleab, P. M. Ajayan, W. Blau, M. Rühle, and D. L. Carroll, Nano Lett. **1**, 457 (2001).
147. J. Liu, S. Webster, and D. L. Carroll, Appl. Phys. Lett. **88**, 213119 (2006)
148. M. Doytcheva, M. Kaiser, M. A. Verheijen, M. Reyes-Reyes, M. Terrones, and N. de Jonge, Chem. Phys. Lett. **396**, 126 (2004).